

Current carried by evanescent modes and possible device application

Sreemoyee Mukherjee¹, P. Singha Deo¹, and A. M. Jayannavar²

¹ *Unit for Nanoscience and Technology, S.N.Bose National Centre For Basic Sciences
Block-JD, Sector-III, Salt Lake, Kolkata-700098, India*

² *Institute of Physics, Sachivalaya Marg, Bhubaneswar 751005, India.*

(Dated: June 24, 2021)

Quantum tunneling of an electron through a classically forbidden regime has no classical analogue and several aspects of it are still not well understood. In this work we analyze electronic currents under the barrier. For this we consider a multichannel Aharonov-Bohm ring and develop a correct formalism to calculate the currents inside the ring when the states are evanescent. We also show unlike other proposed quantum devices that such currents and associated conductance are not very sensitive to changes in material parameters and thus the system can be used to build stable devices that work on magnetic and transport properties. We also study the current magnification property of the ring in presence of both propagating and evanescent states.

I. INTRODUCTION

In the last few decades, there has been a major interest in the area of mesoscopic systems¹. Most of the experimental and theoretical studies of these systems have involved transport measurements, usually of the resistance as a function of temperature or magnetic field. However, there is increasing interest in other non-transport properties, such as magnetization²⁻⁴. This has prompted a lot of experimental works, including the study of arrays of mesoscopic systems^{2,3}, and the use of very small Hall sensors and microsquid magnetometers⁵. These studies give us a unique opportunity to understand and explore manifestations of quantum mechanics like persistent currents⁶, circulating currents⁷ etc.

Mesoscopic structures have led to the possibility of new semiconductor devices. These quantum devices rely on quantum effects for their operation based on quantum interferometric principles, and are quantum analogs of well-known optical and microwave devices⁸. Several potential magnetic devices have been proposed⁹, viz., Hall devices, magnetoresistors, inductive proximity and distance sensors, fluxgate sensors, other magnetic sensors such as magnetodiodes, magFETs, magnetotransistors and carrier domain magnetometers. Some commonly seen devices that work in classical regime and use magnetic properties are magnetic tape used for data storage, magnetic card reader, keycard lock etc. The conventional devices operate in a classical diffusive regime and are not very sensitive to variations in material parameters such as dimensions or the presence of small impurities or non-uniformity in size and shape. These devices operate by controlling the carrier density of quasi-particles. So far no quantum devices in mesoscopic or nanoscopic length have been achieved practically because quantum devices have an inherent shortcoming. Proposed quantum devices are not very robust in the sense that the operational characteristics depend very sensitively on material parameters, impurity configuration, shape and size of sample, temperature and Fermi energy¹⁰. For example, incorporation of a single impurity in the mesoscopic device can change, non-trivially, the interference of par-

tial electron waves propagating through the sample, and hence the electron transmission (operational characteristics) across the sample¹¹. In such devices the actual problem of control and reproducibility of operating thresholds become highly nontrivial. These devices can be exploited if we achieve the technology that can reduce or control the phase fluctuations¹² to a small fraction of 2π . Devices in which electrons carry current without being scattered either elastically or inelastically (ballistic devices) promise to be much faster and will consume less power than the conventional devices. It should also be noted that quantum devices can exhibit multifunctional property (e.g., single stage frequency multiplier) wherein the functions of an entire circuit within a single element can be performed¹³. They can also lead to down sizing of electronic devices.

The conductance of a quantum ring is an oscillating function of magnetic flux through the ring implying we can use flux to drive the system from a conducting state to an insulating state which can be identified as 1 and 0 of a switch as will be exemplified. Such a switch will therefore be working entirely on quantum interference principles which is a new idea in electronic application. Several potential switching devices have been proposed, wherein one controls the relative phase difference between different interfering paths (in semiconducting loop structure) by applying electrostatic or magnetic fields¹⁴⁻¹⁶. The possibility of achieving such transistor action in T-shaped structure by varying the effective length of the vertical open ended lead has also been explored¹⁷. All these proposed devices has not been practical so far because of the inherent shortcoming of quantum devices discussed above.

The magnetization of the ring can be used to store information just like a spatial array of capacitors store information in present day computers or spatially varying magnetic field in magnetic tapes. There can be an array of many quantum rings of different sizes. These can cause a magnetization which has complex spatial variation. A lot of work has been done in one dimensional quantum rings^{12,18-24}. However, the experimental rings are always two dimensional or three dimensional.

Such systems have not received much theoretical attention because multichannel junctions are very difficult to treat theoretically. Open rings where particle exchange can occur and temperature can be defined is more general as closed ring properties can be seen as a special case²⁵. This will be more realistic to study. Besides, open rings can exhibit some novel properties like current magnification or evanescent modes that have no analogs in closed systems. Current magnification is the phenomenon where due to quantum interference large current can circulate in a loop. Circulating currents (or heat current magnification) can also arise in classical coupled oscillator loops²⁶. Spin current magnification can also exhibit magnification effect²⁷. Earlier models either do not account for channel mixing or do not allow the inclusion of evanescent modes. In our present work we account for both of these allowing us to study evanescent states in realistic quasi one-dimensional systems. We show that magnetization due to such evanescent states have very interesting manifestation of quantum effects. We also argue that such effects can be used to build stable devices that uses quantum interference effects. We also study current magnification effect.

II. THEORETICAL ANALYSIS

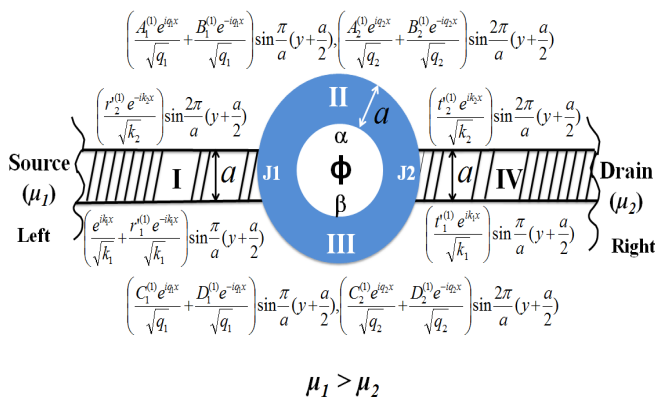


FIG. 1. A finite thickness quantum ring of width a made up of normal metal or semiconductor is indicated by the grey region. On either sides the quantum ring is attached with quantum wires (stripped region) made up of normal metal or semiconductor. On the left of the above system there is the source reservoir whose chemical potential is μ_1 and on the right there is the drain reservoir whose chemical potential is μ_2 . A potential difference $(\mu_1 - \mu_2)$ drives transport currents through the system. The wave functions of the electron in different regions is shown in the figure at their respective places. Different regions are marked as I, II, III and IV. The ring is pierced by an Aharonov-Bohm (A-B) flux ϕ . α is the A-B phase an electron picks up in region II and β is that in region III. J1 is the junction where the regions I, II and III meet and J2 is the junction where the regions II, III and IV meet.

Fig. 1 represents the schematic diagram of a quantum circuit consisting of a ring geometry, made of finite thickness quantum wires. Such quantum wires act like a waveguide^{28,29}. Electronic transport in such systems can be well described by an effective mass theory⁸. Incident electrons coming from the source reservoir on the left (say), gets scattered by the ring. Division of wave front occurs at junction J1; a partial wave propagates along the upper arm of the ring and another partial wave propagates along the lower arm of the ring. These two partial waves recombine and give a transmittance that bears the signature of interference between the two partial waves along the two arms of the ring. This interference can be modified by an Aharonov-Bohm (A-B) flux through the center of the ring. The description of the figure is given in further detail in the figure caption.

The Schrödinger equation for a quasi one dimensional wire is (the third degree of freedom, i.e., z -direction, is usually frozen by creating a strong quantization⁸)

$$-\frac{\hbar^2}{2m^*} \left(\frac{\partial^2 \psi}{\partial x^2} + \frac{\partial^2 \psi}{\partial y^2} \right) + V(x, y) \psi(x, y) = E \psi(x, y) \quad (1)$$

Here the x coordinate is along the wire, y coordinate is perpendicular to it, m^* is the electron effective mass and E is the electron energy. In regions I and IV (see Fig. 1) we have only the confinement potential. That is

$$V(x, y) = V(y).$$

Whereas in regions II and III apart from the confinement potential we take a constant potential V_0 that can be used to excite evanescent modes inside the ring. That is

$$V(x, y) = V(y) + V_0$$

Without any loss of generality we take $V(y)$ to be an infinite square well potential of width a . That is

$$V(y) = \begin{cases} 0 & \text{if } -a/2 < y < a/2; \\ \infty & \text{if } |y| \geq a/2. \end{cases}$$

The wave functions in the ring can be obtained by solving Eq. (1) where we assume the ring to be so large compared to the de Broglie wave length that its curvature can be neglected³⁰. The length of the ring is $L = l_U + l_L$, where l_U is the length of the upper arm and l_L is the length of the lower arm. The magnetic field appears just as a phase of $\psi(x, y)$ and will be accounted for while applying the boundary conditions³¹. In regions I and IV Eq. (1) can be separated as

$$\psi(x, y) = \phi(x) \xi(y) \quad (2)$$

to give

$$-\frac{\hbar^2}{2m^*} \frac{\partial^2 \phi(x)}{\partial x^2} = \frac{\hbar^2 k^2}{2m^*} \phi(x) \quad (3)$$

and

$$-\frac{\hbar^2}{2m^*} \frac{\partial^2 \xi(y)}{\partial y^2} + V(y) \xi(y) = \varepsilon \xi(y) \quad (4)$$

Since $V(y)$ is an infinite square well potential of width a , Eq. (4) gives

$$\xi_n(y) = \sin \frac{n\pi}{a} \left(\frac{a}{2} + y \right) \quad (5)$$

and

$$\varepsilon_n = \frac{n^2 \pi^2 \hbar^2}{2m^* a^2} \quad (6)$$

Eq. (3) has solution of the form

$$\phi_n(x) = e^{\pm i k_n x}$$

with

$$k_n = \sqrt{\frac{2m^* E}{\hbar^2} - \frac{n^2 \pi^2}{a^2}} \quad (7)$$

or

$$E = \varepsilon_n + \frac{\hbar^2 k_n^2}{2m^*} \quad (8)$$

So wave function in region I for electrons incident along channel 1 on the left and electrons are also reflected back to channel 1 on the left, can be written as

$$\psi(I)_1^{(1)} = \left(\frac{e^{i k_1 x}}{\sqrt{k_1}} + \frac{r_1^{(1)} e^{-i k_1 x}}{\sqrt{k_1}} \right) \sin \frac{\pi}{a} \left(y + \frac{a}{2} \right) \quad (9)$$

Wave function in region I for electrons incident along channel 1 on the left and electrons are reflected back to channel 2 on the left, can be written as

$$\psi(I)_2^{(1)} = \left(\frac{r_2^{(1)} e^{-i k_2 x}}{\sqrt{k_2}} \right) \sin \frac{2\pi}{a} \left(y + \frac{a}{2} \right) \quad (10)$$

Wave function in region IV for electrons incident along channel 1 on the left and electrons are transmitted to channel 1 on the right can be written as

$$\psi(IV)_1^{(1)} = \left(\frac{t_1^{(1)} e^{i k_1 x}}{\sqrt{k_1}} \right) \sin \frac{\pi}{a} \left(y + \frac{a}{2} \right) \quad (11)$$

Wave function in region IV for electrons incident along channel 1 on the left and electrons are transmitted to channel 2 on the right can be written as

$$\psi(IV)_2^{(1)} = \left(\frac{t_2^{(1)} e^{i k_2 x}}{\sqrt{k_2}} \right) \sin \frac{2\pi}{a} \left(y + \frac{a}{2} \right) \quad (12)$$

From Eq. (7), in the first mode

$$k_1 = \sqrt{\frac{2m^* E}{\hbar^2} - \frac{\pi^2}{a^2}} \quad (13)$$

is the propagating wave vector and in the second mode

$$k_2 = \sqrt{\frac{2m^* E}{\hbar^2} - \frac{4\pi^2}{a^2}} \quad (14)$$

is the propagating wave vector. For

$$\frac{4\pi^2}{a^2} < E < \frac{9\pi^2}{a^2} \quad (15)$$

both k_1 and k_2 are real as can be seen from Eq. (13) and Eq. (14). In this energy range k_n for $n > 2$ are imaginary as can be seen from Eq. (7) implying that there are two propagating channels. In the leads we can not have evanescent modes^{32,33}.

Now for the regions II and III the potential is $V(x, y) = V(y) + V_0$. In these regimes using q_n as wave vector, the energy can be written similarly like region I and IV as follows

$$E - V_0 = \frac{\hbar^2 q_n^2}{2m^*} + \frac{n^2 \pi^2 \hbar^2}{2m^* a^2} \quad (16)$$

or

$$q_n = \sqrt{\frac{2m^*(E - V_0)}{\hbar^2} - \frac{n^2 \pi^2}{a^2}}$$

Hence, in the first mode

$$q_1 = \sqrt{\frac{2m^*(E - V_0)}{\hbar^2} - \frac{\pi^2}{a^2}} \quad (17)$$

is the wave vector and in the second mode

$$q_2 = \sqrt{\frac{2m^*(E - V_0)}{\hbar^2} - \frac{4\pi^2}{a^2}} \quad (18)$$

is the wave vector. In regions II and III, three different situations can arise depending on the choice of energy, E , potential V_0 and n . Wave functions in these regimes for $E > V_0 + \frac{n^2 \pi^2 \hbar^2}{2m^* a^2}$ can be written similarly as in Eq. (9) - Eq. (12).

$$\psi(II)_1^{(1)} = \left(\frac{A_1^{(1)} e^{i q_1 x}}{\sqrt{q_1}} + \frac{B_1^{(1)} e^{-i q_1 x}}{\sqrt{q_1}} \right) \sin \frac{\pi}{a} \left(y + \frac{a}{2} \right) \quad (19)$$

$$\psi(II)_2^{(1)} = \left(\frac{A_2^{(1)} e^{i q_2 x}}{\sqrt{q_2}} + \frac{B_2^{(1)} e^{-i q_2 x}}{\sqrt{q_2}} \right) \sin \frac{2\pi}{a} \left(y + \frac{a}{2} \right) \quad (20)$$

$$\psi(III)_1^{(1)} = \left(\frac{C_1^{(1)} e^{i q_1 x}}{\sqrt{q_1}} + \frac{D_1^{(1)} e^{-i q_1 x}}{\sqrt{q_1}} \right) \sin \frac{\pi}{a} \left(y + \frac{a}{2} \right) \quad (21)$$

$$\psi(III)_2^{(1)} = \left(\frac{C_2^{(1)} e^{i q_2 x}}{\sqrt{q_2}} + \frac{D_2^{(1)} e^{-i q_2 x}}{\sqrt{q_2}} \right) \sin \frac{2\pi}{a} \left(y + \frac{a}{2} \right) \quad (22)$$

$A_1^{(1)}$, $B_1^{(1)}$, $A_2^{(1)}$, $B_2^{(1)}$ are the amplitudes of wave functions in upper arm and $C_1^{(1)}$, $D_1^{(1)}$, $C_2^{(1)}$, $D_2^{(1)}$ are the amplitudes of wave functions in lower arm for incidence of electrons along channel 1. Similarly, $A_1^{(2)}$, $B_1^{(2)}$, $A_2^{(2)}$, $B_2^{(2)}$ are the amplitudes of wave functions in upper arm

and $C_1^{(2)}$, $D_1^{(2)}$, $C_2^{(2)}$, $D_2^{(2)}$ are the amplitudes of wave functions in lower arm for incidence of electrons along channel 2. Depending on the choice of energy E and potential V_0 , q_1 and q_2 can be real (propagating mode) as well as imaginary (evanescent mode). Such evanescent states can always be excited in the internal regions of the system but not in leads^{32,33}. In the regimes II and III, we can choose V_0 to be non-zero such that for $n = 1, 2$, $E < V_0 + \frac{n^2\pi^2\hbar^2}{2m^*a^2}$. Then we are considering both channels (modes) to be evanescent. For such evanescent channels q_n in Eq. (19) and Eq. (22) is replaced by is_n and wave functions can be written as

$$\psi(II)_1^{(1)} = \left(\frac{A_1^{(1)} e^{-s_1 x}}{\sqrt{is_1}} + \frac{B_1^{(1)} e^{s_1 x}}{\sqrt{is_1}} \right) \sin \frac{\pi}{a} \left(y + \frac{a}{2} \right) \quad (23)$$

$$\psi(II)_2^{(1)} = \left(\frac{A_2^{(1)} e^{-s_2 x}}{\sqrt{is_2}} + \frac{B_2^{(1)} e^{s_2 x}}{\sqrt{is_2}} \right) \sin \frac{2\pi}{a} \left(y + \frac{a}{2} \right) \quad (24)$$

$$\psi(III)_1^{(1)} = \left(\frac{C_1^{(1)} e^{-s_1 x}}{\sqrt{is_1}} + \frac{D_1^{(1)} e^{s_1 x}}{\sqrt{is_1}} \right) \sin \frac{\pi}{a} \left(y + \frac{a}{2} \right) \quad (25)$$

$$\psi(III)_2^{(1)} = \left(\frac{C_2^{(1)} e^{-s_2 x}}{\sqrt{is_2}} + \frac{D_2^{(1)} e^{s_2 x}}{\sqrt{is_2}} \right) \sin \frac{2\pi}{a} \left(y + \frac{a}{2} \right) \quad (26)$$

Note that this form of the wave functions along with its imaginary normalization constant is necessary to give the correct expression for currents in evanescent modes. We can also choose the constant potential V_0 and the n value of $\frac{n^2\pi^2\hbar^2}{2m^*a^2}$ in such a fashion that one channel (or mode) is propagating and the other channel (or mode) is evanescent and we can describe the wavefunctions appropriately.

In Fig. 1 the potential V_0 in the shaded region need not be made by an electrostatic field. One can do it by designing the system as shown in Fig. 2. Fig. 2 represents the schematic diagram of a mesoscopic interferometer (made up of normal metal or semiconductor). The width of the quantum wire a , is greater than the width of quantum ring w . Electrostatic potential is 0 everywhere. For the regions II and III in Fig. 2, one can obtain just like in Eq. (17) and (18),

$$\begin{aligned} q'_1 &= \sqrt{\frac{2m^*E}{\hbar^2} - \frac{\pi^2}{w^2}} \\ &= \sqrt{\frac{2m^*E}{\hbar^2} - \frac{\pi^2}{a^2} + \frac{\pi^2}{a^2} - \frac{\pi^2}{w^2}} \\ &= \sqrt{\frac{2m^*(E - V'_0)}{\hbar^2} - \frac{\pi^2}{a^2}} \end{aligned} \quad (27)$$

where $\frac{\pi^2}{a^2} - \frac{\pi^2}{w^2} = -\frac{2m^*V'_0}{\hbar^2}$. Similarly, in the second mode

$$q'_2 = \sqrt{\frac{2m^*(E - V''_0)}{\hbar^2} - \frac{4\pi^2}{a^2}} \quad (28)$$

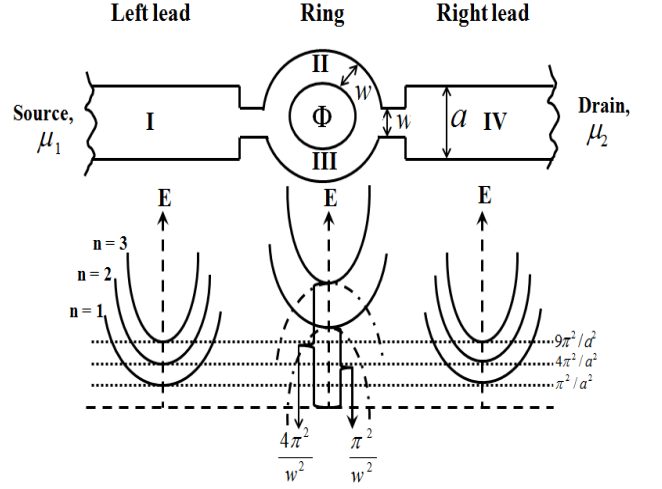


FIG. 2. Top: Schematic diagram of another mesoscopic interferometer coupled to the left and right electron reservoirs. Electrostatic potential is zero everywhere. Bottom: Energy level dispersion curve for each region. Dispersion relation, $E(k_n)$ vs. k_n obtained from Eq. (8) for propagating modes in regions I and IV, indicated by solid lines. Dispersion relation, $E(q'_n)$ vs. q'_n obtained from Eq. (27) and Eq. (28) for propagating modes in regions II and III, indicated by solid lines. Dispersion relation, $E(s_n)$ vs. s_n obtained from Eq. (29) and Eq. (30) for evanescent modes in regions II and III, indicated by dash-dotted lines.

where $\frac{4\pi^2}{a^2} - \frac{4\pi^2}{w^2} = -\frac{2m^*V''_0}{\hbar^2}$. Therefore, V'_0 and V''_0 play the same role as V_0 in Eq. (17) and (18). However, it simply originates from geometric parameters and not from an electrostatic potential. The dispersion relation $E(S_n)$ for the evanescent mode wavefunctions (Eq. (23) and (26)) in regions II and III can also be obtained from Eq. (27) and Eq. (28) using the fact $q'_n \rightarrow is_n$. Therefore, they are given by

$$s_1 = \sqrt{\frac{\pi^2}{w^2} - \frac{2m^*E}{\hbar^2}} \quad (29)$$

$$s_2 = \sqrt{\frac{4\pi^2}{w^2} - \frac{2m^*E}{\hbar^2}} \quad (30)$$

The dispersion relations for different regions (I, II and III, IV) are also shown in Fig. 2. In regions I and IV, from Eq. (8) we see that E is given by $E(k_n) = \frac{\hbar^2 k_n^2}{2m^*} + \frac{n^2\pi^2\hbar^2}{2m^*a^2}$, where $n = 1, 2, 3, \dots$, denotes the modes. These dispersion relations for different modes indexed by n are indicated by solid lines (see Fig. 2). The offset values are obtained at $\frac{\pi^2}{a^2}$ (for $n = 1$), $\frac{4\pi^2}{a^2}$ (for $n = 2$) etc and are indicated by dotted lines. In regions II and III, $E(q'_n)$ is given by Eq. (27) and Eq. (28) and the offset is $\frac{\pi^2}{w^2}$ and $\frac{4\pi^2}{w^2}$ for the two modes shown ($n = 1$ and $n = 2$). Here the offset values are indicated by the second brackets. There are no propagating states between the dotted

lines at $\frac{\pi^2}{a^2}$ (for $n = 1$) and $\frac{9\pi^2}{a^2}$ (for $n = 3$) within the ring but there are propagating states in the leads. In these energy regimes, the electrons tunnel through as evanescent modes described by Eq. (23) - Eq. (26). Their dispersion curve $E(s_n)$ as obtained from Eq. (29) and Eq. (30) are shown by dash-dotted lines.

Note that a two dimensional quantum wire can be also converted into a Aharonov-Bohm set up as shown in Fig. 3. Essentially one can form a cylinder that can enclose a flux³⁴. In this case all the analysis given above remains the same. For example if now we choose cylindrical co-

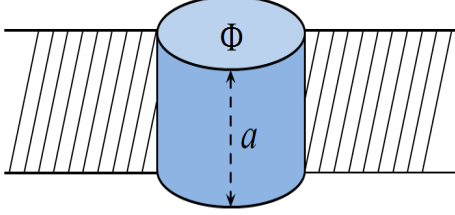


FIG. 3. Cylindrical Aharonov-Bohm set up

ordinates the wave function in Eq. (19) becomes

$$\psi_{(II)_1}^{(1)} = \left(\frac{A_1^{(1)} e^{im_1\theta}}{\sqrt{m_1}} + \frac{B_1^{(1)} e^{-im_1\theta}}{\sqrt{m_1}} \right) \sin \frac{\pi}{a} \left(z + \frac{a}{2} \right) \quad (31)$$

In fact this makes analysis much simpler because m_1 stands for angular momentum and takes into account the curvature of the ring. The advantage of this set up is already described by S. Mukherjee et al.³⁵.

In our previous work³⁵ we proposed a junction scattering matrix S for a multi-channel junction that can be easily generalized to any number of channels. One can match the wave functions depicted in Fig. 1 at junction J1 and J2 and conserve the currents by using these S -matrices that give us a set of linear equations. For evanescent modes the internal wavefunctions has to be appropriately chosen, given by Eq. (23) - Eq. (26). We can calculate the coefficients $A_1^{(1)}, A_2^{(1)}, B_1^{(1)}, B_2^{(1)}, A_1^{(2)}, A_2^{(2)}, B_1^{(2)}, B_2^{(2)}, C_1^{(1)}, C_2^{(1)}, D_1^{(1)}, D_2^{(1)}, C_1^{(2)}, C_2^{(2)}, D_1^{(2)}$ and $D_2^{(2)}$ by matrix inversion.

The general definition of current (I) is given by

$$I = \int_{-\frac{a}{2}}^{\frac{a}{2}} \frac{e\hbar}{2im^*} (\Psi^\dagger \vec{\nabla} \Psi - \Psi \vec{\nabla} \Psi^\dagger) dy \quad (32)$$

Suppose there are two channels (modes) in the ring, which are both propagating. Current (I) in propagating mode is obtained by calculating Eq. (32) for wave functions given by equations from Eq. (19) to Eq. (22). For such propagating modes in upper arm, for incidence along channel 1, the partial current is given by

$$I_U^{(1)}(pp) = \frac{e\hbar}{m^*} [|A_1^{(1)}|^2 - |B_1^{(1)}|^2 + |A_2^{(1)}|^2 - |B_2^{(1)}|^2] \quad (33)$$

For propagating modes in upper arm, for incidence along channel 2, the partial current is given by

$$I_U^{(2)}(pp) = \frac{e\hbar}{m^*} [|A_1^{(2)}|^2 - |B_1^{(2)}|^2 + |A_2^{(2)}|^2 - |B_2^{(2)}|^2] \quad (34)$$

Similarly, for propagating modes in lower arm, for incidence along channel 1 and 2, the partial currents are given by

$$I_L^{(1)}(pp) = \frac{e\hbar}{m^*} [|C_1^{(1)}|^2 - |D_1^{(1)}|^2 + |C_2^{(1)}|^2 - |D_2^{(1)}|^2] \quad (35)$$

and

$$I_L^{(2)}(pp) = \frac{e\hbar}{m^*} [|C_1^{(2)}|^2 - |D_1^{(2)}|^2 + |C_2^{(2)}|^2 - |D_2^{(2)}|^2] \quad (36)$$

When both modes are propagating using Eqs. (33) and (34) we can write the net current in upper arm as

$$I_U = I_U^{(1)}(pp) + I_U^{(2)}(pp) \quad (37)$$

When both modes are propagating using Eqs. (35) and (36) we can write the net current in lower arm as

$$I_L = I_L^{(1)}(pp) + I_L^{(2)}(pp) \quad (38)$$

Next we consider that there are two channels (modes) in the ring, one being propagating and other being evanescent. Current (I) using one propagating mode and one evanescent mode is obtained by calculating Eq. (32) choosing the wavefunctions appropriately for propagating mode and evanescent mode given in Eq. (19) to Eq. (26). In this case in upper arm for incidence along channel 1 the partial current is given by

$$I_U^{(1)}(pe) = \frac{e\hbar}{m^*} [|A_1^{(1)}|^2 - |B_1^{(1)}|^2] + \frac{e\hbar}{im^*} [A_2^{(1)*} B_2^{(1)} e^{-i\alpha} - A_2^{(1)} B_2^{(1)*} e^{i\alpha}] \quad (39)$$

For one propagating mode and one evanescent mode in upper arm, for incidence along channel 2, the partial current is given by

$$I_U^{(2)}(pe) = \frac{e\hbar}{m^*} [|A_1^{(2)}|^2 - |B_1^{(2)}|^2] + \frac{e\hbar}{im^*} [A_2^{(2)*} B_2^{(2)} e^{-i\alpha} - A_2^{(2)} B_2^{(2)*} e^{i\alpha}] \quad (40)$$

Similarly, for one propagating mode and one evanescent mode in lower arm, for incidence along channel 1 and 2, the partial currents are given by

$$I_L^{(1)}(pe) = \frac{e\hbar}{m^*} [|C_1^{(1)}|^2 - |D_1^{(1)}|^2] + \frac{e\hbar}{im^*} [C_2^{(1)*} D_2^{(1)} e^{-i\alpha} - C_2^{(1)} D_2^{(1)*} e^{i\alpha}] \quad (41)$$

and

$$I_L^{(2)}(pe) = \frac{e\hbar}{m^*} [|C_1^{(2)}|^2 - |D_1^{(2)}|^2] + \frac{e\hbar}{im^*} [C_2^{(2)*} D_2^{(2)} e^{-i\beta} - C_2^{(2)} D_2^{(2)*} e^{i\beta}] \quad (42)$$

For using one propagating mode and one evanescent mode the net current in upper arm is given by

$$I_U = I_U^1(pe) + I_U^2(pe) \quad (43)$$

For using one propagating mode and one evanescent mode the net current in lower arm is given by

$$I_L = I_L^1(pe) + I_L^2(pe) \quad (44)$$

Next we consider that both the channels are evanescent. The current (I) for two evanescent modes is obtained by calculating Eq. (32) choosing the wavefunctions appropriately for evanescent modes given in Eq. (23) to Eq. (26). For such evanescent modes the partial current in upper arm, for incidence along channel 1 is given by

$$I_U^{(1)}(ee) = \frac{e\hbar}{im^*} [A_1^{(1)*} B_1^{(1)} e^{-i\alpha} - A_1^{(1)} B_1^{(1)*} e^{i\alpha} + A_2^{(1)*} B_2^{(1)} e^{-i\alpha} - A_2^{(1)} B_2^{(1)*} e^{i\alpha}] \quad (45)$$

For evanescent mode the partial current in upper arm, for incidence along channel 2 is given by

$$I_U^{(2)}(ee) = \frac{e\hbar}{im^*} [A_1^{(2)*} B_1^{(2)} e^{-i\alpha} - A_1^{(2)} B_1^{(2)*} e^{i\alpha} + A_2^{(2)*} B_2^{(2)} e^{-i\alpha} - A_2^{(2)} B_2^{(2)*} e^{i\alpha}] \quad (46)$$

Similarly, for evanescent mode in lower arm and incidence along channel 1 and 2, the partial currents are given by

$$I_L^{(1)}(ee) = \frac{e\hbar}{im^*} [C_1^{(1)} D_1^{(1)*} e^{i\beta} - C_1^{(1)*} D_1^{(1)} e^{-i\beta} + C_2^{(1)} D_2^{(1)*} e^{i\beta} - C_2^{(1)*} D_2^{(1)} e^{-i\beta}] \quad (47)$$

and

$$I_L^{(2)}(ee) = \frac{e\hbar}{im^*} [C_1^{(2)} D_1^{(2)*} e^{i\beta} - C_1^{(2)*} D_1^{(2)} e^{-i\beta} + C_2^{(2)} D_2^{(2)*} e^{i\beta} - C_2^{(2)*} D_2^{(2)} e^{-i\beta}] \quad (48)$$

From Eqs. (45) and (46) we can write for evanescent modes the net current in upper arm is given by

$$I_U = I_U^{(1)}(ee) + I_U^{(2)}(ee) \quad (49)$$

Similarly, from Eqs. (47) and (48) we can write for evanescent modes net current in lower arm is given by

$$I_L = I_L^{(1)}(ee) + I_L^{(2)}(ee) \quad (50)$$

III. RESULTS AND DISCUSSIONS

A. Conductance of a multi-channel A-B ring

We are considering a two channel A-B ring that is characterized by four transmission amplitudes $t_1^{(1)}$, $t_2^{(1)}$, $t_1^{(2)}$ and $t_2^{(2)}$ and four reflection amplitudes $r_1^{(1)}$, $r_2^{(1)}$, $r_1^{(2)}$

and $r_2^{(2)}$. Landauer's formula gives the two probe conductance G as

$$G = \frac{2e^2}{h} \sum_{i,j} |t_j^{(i)}|^2. \quad (51)$$

The transmission amplitude from mode i to mode j is $t_j^{(i)}$. G is a strongly oscillating function of ϕ/ϕ_0 implying we can use flux to drive the system from a conducting state to an insulating state. In case of a triode, we can use grid voltage to change the current flow from cathode to anode and therefore use it as a switch or a transistor. Similarly, in this A-B set up we can use magnetic field to control the current from source to drain and similarly we can use it as a switch or a transistor.

In an A-B ring, switching action is based on constructive and destructive interference and is extremely sensitive to small changes in parameters like Fermi energy, ring length, arm lengths etc. They are practically impossible to control¹⁰. This fact changes completely if we use evanescent modes³⁵. An electron in an evanescent mode do not acquire phase changes associated with propagation or impurity scattering. Only phase changes are due to A-B effect and we find that within a period (0 to 2π) conductance is maximum (or minimum) at zero flux, then it goes through a deep minimum (or a maximum) and rises (or falls) again to a maximum (or minimum) value. One can explain this as follows. Conductance being a symmetric function of flux (Onsager reciprocity relation), is a function of $(\cos n\phi/\phi_0)$. So it maximizes (or minimizes) at 0 flux and then decreases (or increases) with flux. Periodicity is always ϕ_0 in absence of other competing source of phase changes and absence of resonance. This behavior is independent of all parameters. Since evanescent modes are not very conducting we have to take smaller rings. A plot of the conductance is shown in Fig. 4 that exhibits this.

B. Circulating currents in a multi-channel A-B ring

Let us consider the system in absence of flux. When $l_U = l_L$, the currents I_S through the system (source to drain currents) split at junction J1 and divides into two equal parts. The upper arm current, I_U (i.e., $I_S/2$) flows in clockwise direction along the upper arm of the ring and the lower arm current, I_L (i.e., $I_S/2$) flows in anti-clockwise direction along the lower arm of the ring. The clockwise and anti-clockwise currents are equal in magnitude and hence the system has no magnetization. When $l_U \neq l_L$, in absence of flux, these two currents are different in magnitude and there exists two distinct possibilities depending on the choice of l_U , l_L ($l_U \neq l_L$) and Fermi energy. In the first possibility, for a certain range of incident Fermi energies (or wave vectors), the currents in the two arms I_U and I_L are individually less than I_S . Then currents in both arms flow in the direction of the chemical potential gradient, upper arm current flows in clockwise

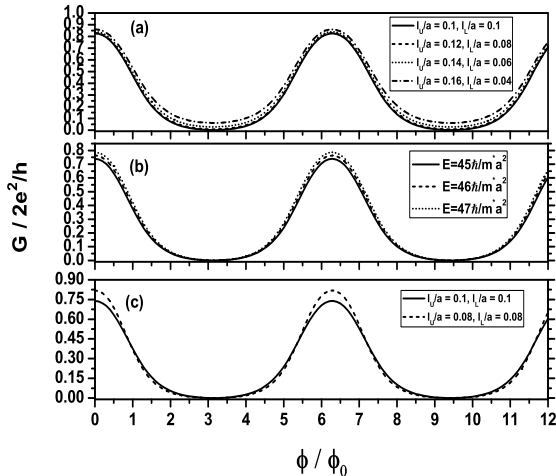


FIG. 4. The figures (a) - (c) show plots of conductance, $G/2e^2/h$ as a function of ϕ/ϕ_0 using evanescent modes for different arm lengths (a), for different Fermi energy (b) and for different ring lengths (c). Here $\phi_0 = hc/e$. The exact values of Em^*a^2/h^2 , l_U and l_L are given in the figure inset. For all sets of different parameters $G/2e^2/h$ as a function of ϕ/ϕ_0 have the same nature.

direction and lower arm current flows in anti-clockwise direction. In such a situation there is no circulating currents flowing in the ring. However, in a certain energy interval, it turns out that current in one arm (upper or lower) is larger than the total currents I_S (magnification property). This implies that, to conserve the total currents at the junctions, the current in the other arm (lower or upper) should flow against the chemical potential gradient. In such a situation the current flow in this arm of the loop continues to flow in the ring as a circulating currents. Based on the constraints on the local currents, the existence of circulating currents in a one-dimensional mesoscopic ring with asymmetric arm lengths was established in earlier works^{7,37,38}. In 2010, Su et. al.³⁹ formulated the constraint condition for circulating currents as follows:

$$I_c = \frac{1}{2} \text{sign}[I_U](|I_U| + |I_L| - I_S) \quad (52)$$

In presence of flux, the circulating currents I_c changes drastically in magnitude but the definition remains the same. Once we have formalized the current flowing in the multichannel quasi one-dimensional ring we can use the same definition to calculate the circulating currents I_c in the system shown in Fig. 1. We now plot circulating currents as well as transmission coefficient as a function of incident Fermi energy for this system.

Two propagating modes: We first consider a case when both the channels (modes) in the ring are propagating. In Fig. 5 we have plotted the circulating currents I_c (solid curve) as a function of incident Fermi energy. We have taken $l_U/a = 3$ and $l_L/a = 7$. In Fig. 5 we have also

plotted the transmission coefficient $\sum_{i,j} |t_j^{(i)}|^2$ (dashed curve). We notice that the circulating currents appears as we cross the energy where $\sum_{i,j} |t_j^{(i)}|^2 = 0$. In absence of channel mixing $\sum_{i,j} |t_j^{(i)}|^2$ can have minima but does not become 0. Thus inclusion of evanescent mode is very important to study current magnification.

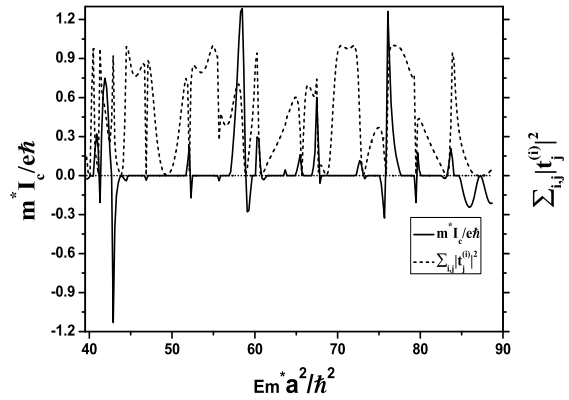


FIG. 5. The figure shows plot of circulating currents (I_c) in dimensionless unit (solid curve) and transmission coefficient ($\sum_{i,j} |t_j^{(i)}|^2$) (dashed curve) as a function of incident Fermi energy using two propagating modes. Here upper arm length, $l_U/a = 3$ and lower arm length, $l_L/a = 7$.

One propagating mode and one evanescent mode: Now we will consider the case where one mode is propagating and the other mode is evanescent. In Fig. 6 we have plotted circulating currents I_c (solid curve) as a function of incident Fermi energy. We have taken $l_U/a = 3$ and $l_L/a = 7$. In Fig. 6 we have also plotted the transmission coefficient, $\sum_{i,j} |t_j^{(i)}|^2$ (dashed curve). We again notice that the circulating currents appear as we cross the energy where $\sum_{i,j} |t_j^{(i)}|^2 = 0$.

When both modes are evanescent then there is no circulating currents in the system. This is essentially because evanescent modes are decaying modes and for such modes I_U or I_L cannot be greater than I_S for any energy.

C. Magnetization of a multi-channel A-B ring

The geometry in consideration (Fig. 1, Fig. 2, Fig. 3) can have a magnetization due to the internal currents in regions II and III. A proper formulation for evaluating such internal currents in the regime of evanescent modes is still not well established^{7,37,38} and the correct formalism that gives consistent results in every situation is given in Eqs. (33) - (50). This internal currents can induce a magnetic field that can be measured.

There are two different origins to this magnetization. First is due to transport currents and this magnetization can be there even in absence of the A-B flux. The

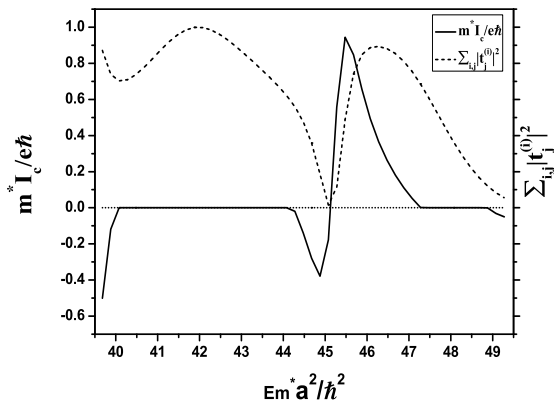


FIG. 6. The figure shows plot of circulating currents (I_c) in dimensionless unit (solid curve) and transmission coefficient ($\sum_{i,j} |t_j^{(i)}|^2$) (dashed curve) as a function of Fermi energy of incident electrons using one propagating mode and one evanescent mode. Here upper arm length, $l_U/a = 3$ and lower arm length, $l_L/a = 7$.

currents through the sample, I_S splits into I_U and I_L in upper arm and lower arm, respectively. For $l_U \neq l_L$, $I_U \neq I_L$ and thus the clockwise current is different from anticlockwise current. This can result in a magnetization, magnetization strength is given by $(I_U \cdot l_U + I_L \cdot l_L)$. The current in lower arm (upper arm), I_L (I_U) by definition is negative (positive). In regimes of circulating currents I_L (I_U) becomes positive (negative) leading to a large enhancement in magnetization which is shown in Fig. 7 where we have plotted magnetization strength as a function of Fermi energy. Flux value is taken to be 0, and there are two propagating modes. The second

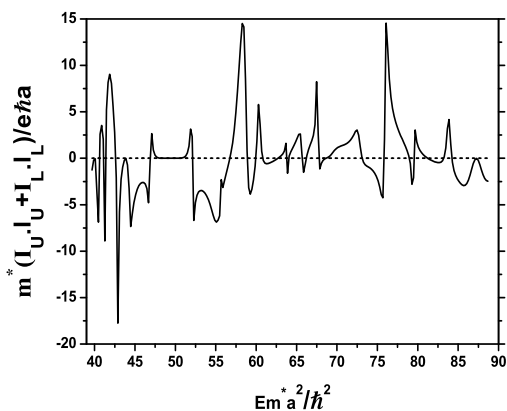


FIG. 7. The figure shows plot of magnetization strength in dimensionless unit as a function of Fermi energy using two propagating modes. Here upper arm length, $l_U/a = 3$ and lower arm length, $l_L/a = 7$.

is due to the A-B flux and this magnetization can exist

even if $\mu_1 = \mu_2$ and there is no incident current. A-B flux induces an equilibrium current and this current is always an odd function of flux⁴⁰. The first kind of magnetization is further modified by the flux but is always an even function of flux. It is known that the odd component can be determined from the even component²⁵ and vice versa. The total magnetization is therefore a linear combination of an even and an odd function of flux and hence can be any arbitrary function of flux. It will be a function of $\cos(n\phi/\phi_0)$ as well as $\sin(n\phi/\phi_0)$. Therefore unlike the conductance it will not maximize (or minimize) at 0 flux and then decreases (or increases) with flux. It can maximize at any arbitrary flux. Therefore it remains to be seen if magnetization due to evanescent modes remain independent of material parameters. If it does then one can build stable devices that rely on magnetization. In practice it is not always possible to maintain either the ring length (or arm length) or the incident energy ($Em^* a^2/\hbar^2$) values constant due to statistical fluctuation or temperature changes.

Two propagating modes: Here we have taken three different cases. In all three cases we have plotted the strength of magnetization, i.e., $(I_U \cdot l_U + I_L \cdot l_L)$ as a function of ϕ/ϕ_0 for different parameters. In the first case we have taken two different arm length values keeping the Fermi energy and total ring length same (see Fig. 8 (a)). In the second case we have taken two different Fermi energy values keeping the ratio of arm length and total ring length same (see Fig. 8 (b)). In the third case we have taken two different ring length values keeping the Fermi energy and ratio of arm length same (see Fig. 8 (c)). The parameter values are described in detail in figure caption. In the first case we can see that the maximum of the solid line and the dashed line are not obtained at the same flux values. In the second case the solid line has no distinct features whereas the dashed line has sharp maximum and minimum. In the third case the maximum and minimum of the solid line are not in the same phase as that of the dashed line. Thus we can see here that the strength of magnetization $(I_U \cdot l_U + I_L \cdot l_L)$ as a function of ϕ/ϕ_0 is strongly dependent on variations in parameters like different ratio of arm lengths, different Fermi energies, different total ring lengths etc. Therefore we can conclude that using propagating modes we can not build reliable devices based on magnetic properties.

One propagating mode and one evanescent mode: Here we have taken three different cases. In all three cases we have plotted the strength of magnetization, i.e., $(I_U \cdot l_U + I_L \cdot l_L)$ as a function of ϕ/ϕ_0 for different parameters. In the first case we have taken two different arm length values keeping the Fermi energy and total ring length same (see Fig. 9 (a)). In the second case we have taken two different Fermi energy values keeping the ratio of arm length and total ring length same (see Fig. 9 (b)). In the third case we have taken two different ring length values keeping the Fermi energy and ratio of arm length same (see Fig. 9 (c)). The parameter values are described in detail in figure caption. In the first case we

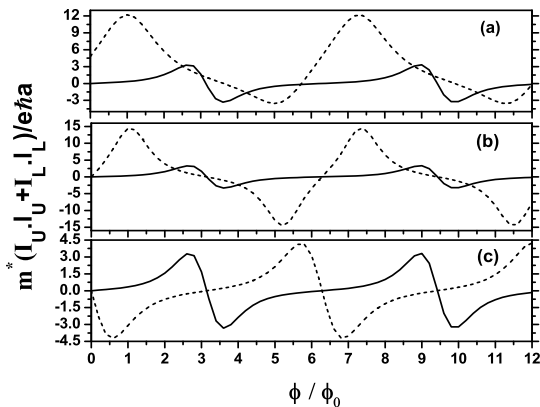


FIG. 8. The figures (a) - (c) show plot of magnetization strength in dimensionless unit for the system in Fig. 1 as a function of ϕ/ϕ_0 for different choice of parameters. Here $\phi_0 = hc/e$. The constant potential V_0 is taken as 0, so that both the modes are propagating. In (a), the incoming electrons have energy $E = \frac{55\hbar^2}{m^*a^2}$. The solid line is for $l_U/a = 5, l_L/a = 5$ and the dashed line is for $l_U/a = 4, l_L/a = 6$. In (b) the arm length ratio is taken as $l_U : l_L = 5 : 5$. The solid line is for $E = \frac{55\hbar^2}{m^*a^2}$ and the dashed line is for $E = \frac{57\hbar^2}{m^*a^2}$. In (c), the incoming electrons have energy $E = \frac{55\hbar^2}{m^*a^2}$. Keeping the arm length ratio same ($l_U : l_L = 1 : 1$) we have taken here different ring lengths. The solid line is for $L/a = 10$ and the dashed line is for $L/a = 8$.

can see that the solid line has no distinct features whereas the dashed line has sharp maximum and minimum. In the second case we can see that where the solid line has minimum the dashed line has maximum and vice versa. In the third case the maximum and the minimum of the solid line are not in the same phase as that of the dashed line. Thus we can see here that the strength of magnetization ($I_U.l_U + I_L.l_L$) as a function of ϕ/ϕ_0 is strongly dependent upon the variations in parameters like different ratio of arm lengths, different Fermi energy, different total ring length etc. Therefore we can conclude that using one propagating mode and one evanescent mode we can not build reliable devices based on magnetic properties.

This random behavior of magnetization is essentially due to extreme sensitivity of quantum interference to small changes in phase of wavefunction. Fig. 8 (a), (b), (c) and Fig. 9 (a), (b), (c) exemplifies this for some representative choice of parameters and can be easily checked for any other choice of parameters.

Two evanescent modes: Here also we have taken three different cases. In all three cases we have plotted the strength of magnetization, i.e., ($I_U.l_U + I_L.l_L$) as a function of ϕ/ϕ_0 for different parameters. In the first case we have taken two different arm length values keeping the Fermi energy and total ring length same (see Fig. 10 (a)). In the second case we have taken two different Fermi energy values keeping the ratio of arm length and

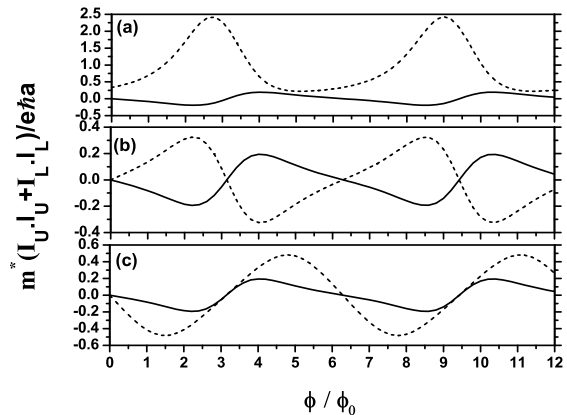


FIG. 9. The figures (a) - (c) show plot of magnetization strength in dimensionless unit for the system in Fig. 1 as a function of ϕ/ϕ_0 . The constant potential V_0 of the ring is such that $V_0 = 10\hbar^2/em^*a^2$. With this choice q_1 is real and q_2 is imaginary. Thus we are considering in this case one propagating mode and one evanescent mode. In (a), the incoming electrons have energy $E = \frac{45\hbar^2}{m^*a^2}$. The solid line is for $l_U/a = 1, l_L/a = 1$ and the dashed line is for $l_U/a = 1.2, l_L/a = 0.8$. In (b) the arm length ratio is taken as $l_U : l_L = 1 : 1$. The solid line is for $E = \frac{45\hbar^2}{m^*a^2}$ and the dashed line is for $E = \frac{47\hbar^2}{m^*a^2}$. In (c), the incoming electrons have energy $E = \frac{45\hbar^2}{m^*a^2}$. Keeping the arm length ratio same ($l_U : l_L = 1 : 1$) we have taken here different ring lengths. The solid line is for $L/a = 2$ and the dashed line is for $L/a = 1.6$.

total ring length same (see Fig. 10 (b)). In the third case we have taken two different ring length values keeping the Fermi energy and ratio of arm length same (see Fig. 10 (c)). The parameter values are described in detail in figure caption. In all three cases we have shown that the strength of magnetization ($I_U.l_U + I_L.l_L$) as a function of ϕ/ϕ_0 is qualitatively as well as quantitatively same for different choice of parameters like different ratio of arm lengths, different Fermi energies, different total ring lengths etc. So there is possibility of robust device action based on magnetic response using only evanescent modes which contradicts earlier works that devices based on quantum interference effects cannot be achieved. Note that the maximum or the minimum in figures (Fig. 10 (a), (b) and (c)) is not at 0 flux as we have argued. However the maxima and minima are fixed and do not change with change in parameters. The reason for this is explained later.

So far we have considered three different cases - (i) keeping Fermi energy value and ring length fixed, we have chosen three different sets of arm lengths, (ii) keeping arm length and ring length fixed, we have chosen three different sets of Fermi energies, and (iii) keeping Fermi energy value and arm length fixed, we have chosen three different sets of ring lengths. In Fig. 11 we will discuss another set of plots where we have chosen incident Fermi energy and electrostatic potential inside the ring in such a fashion that both the channels are evanescent and sam-

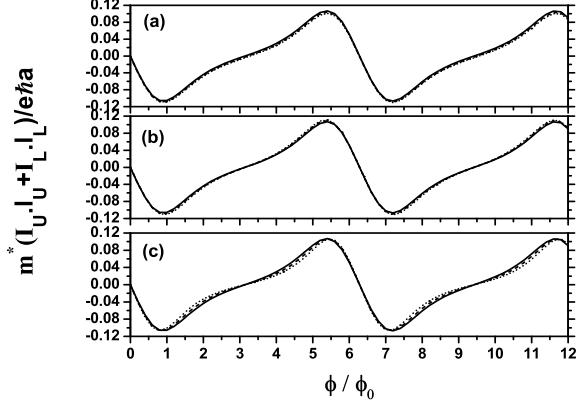


FIG. 10. The figures (a) - (c) show plots of magnetization strength in dimensionless unit for the system in Fig. 1 as a function of ϕ/ϕ_0 for an Aharonov-Bohm interferometer where all the current carrying modes are evanescent. Here $\phi_0 = hc/e$. In (a), the incoming electrons have energy $E = \frac{45\hbar^2}{m^*a^2}$. The solid line is for $l_U/a = 0.1, l_L/a = 0.1$, the dashed line is for $l_U/a = 0.12, l_L/a = 0.08$ and the dotted line is for $l_U/a = 0.14, l_L/a = 0.06$. All three plots show nature of magnetization is independent of relative ratio of arm lengths. In (b), the arm length ratio is taken as $l_U : l_L = 0.1 : 0.1$. The solid line is for $E = \frac{45\hbar^2}{m^*a^2}$, the dashed line is for $E = \frac{46\hbar^2}{m^*a^2}$ and the dotted line is for $E = \frac{47\hbar^2}{m^*a^2}$. All three plots show nature of magnetization is independent of Fermi energy. In (c), the incoming electrons have energy $E = \frac{45\hbar^2}{m^*a^2}$. Keeping the arm length ratio same ($l_U : l_L = 1 : 1$) we have taken here different ring lengths. The solid line is for $L/a = 0.2$, the dashed line is for $L/a = 0.18$ and the dotted line is for $L/a = 0.16$. All three plots show nature of magnetization is independent of total ring length.

ple parameters vary randomly. Sample parameter choice is described in the figure caption. Here too we show that magnetic behavior for random choice of parameters is qualitatively as well as quantitatively the same.

As we have argued before the current in the upper arm (I_U) and that in the lower arm (I_L) has an even (in ϕ) contribution and an odd contribution. This uniform behavior of magnetization can be understood by analyzing the even and odd components separately. The even current is transport current which is given by

$$I_{U,L}^{even} = \frac{I_{U,L}(\phi) + I_{U,L}(-\phi)}{2}$$

and plotted in Fig. 12. In Fig. 12 (a), we have plotted the transport current of the upper arm (I_U^{even}) as a function of flux and in Fig. 12 (b), we have plotted transport current of the lower arm (I_L^{even}) as a function of flux. Keeping the total ring length same we have taken four different choices of arm length ratio and in all four cases we have shown that the nature of the transport currents (in terms of position of maximum and minimum) in both upper arm and lower arm remains the same that is independent of arm length ratio. In both these figures peak value, i.e., I^{max} is obtained at $\phi/\phi_0 = 6.2$. In Fig. 12

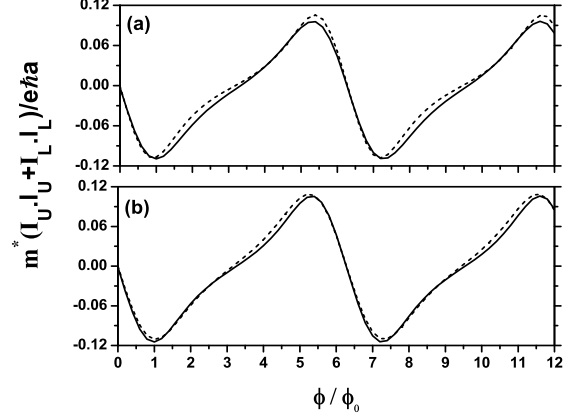


FIG. 11. The figures (a) - (b) show plot of magnetization strength for the system in Fig. 1 as a function of ϕ/ϕ_0 for an Aharonov-Bohm interferometer where all the current carrying modes are evanescent. Here $\phi_0 = hc/e$. In (a), the incoming electrons have energy $E = \frac{45\hbar^2}{m^*a^2}$. The solid line is for $L/a = 0.24$ and the dashed line is for $l_U/a = 0.11, l_L/a = 0.09$. In (b), the incoming electrons have energy $E = \frac{47\hbar^2}{m^*a^2}$. The solid line is for $L/a = 0.22$ and the dashed line is for $l_U/a = 0.13, l_L/a = 0.12$. Here (a) and (b) shows that plots are independent of material parameters.

(a), with the increasing value of the upper arm length the I_U^{max} value decreases and in Fig. 12 (b), with the decreasing value of the lower arm length the I_L^{max} value increases.

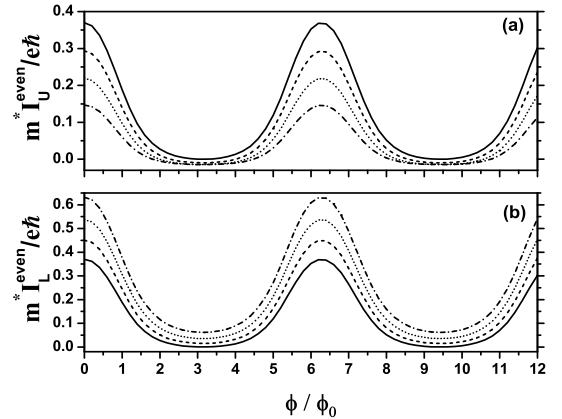


FIG. 12. The figures (a) - (b) show plots of transport currents $I_{U/L}^{even}$ in dimensionless unit for the system in Fig. 1 as a function of ϕ/ϕ_0 for different arm lengths keeping the ring length same. In (a) and (b), the solid line is for arm length values of $l_U/a = 0.1, l_L/a = 0.1$, the dashed line is for arm length values of $l_U/a = 0.12, l_L/a = 0.08$, the dotted line is for arm length values of $l_U/a = 0.14, l_L/a = 0.06$, and the dash-dotted line is for arm length values of $l_U/a = 0.16, l_L/a = 0.04$.

One would have thought that since the evanescent modes decay exponentially inside the barrier, $I_{U/L}^{max}$ would

have scaled exponentially with the length. But counter-intuitively they scale linearly. The peak value ($I_{U/L}^{max}$), obtained at $\phi/\phi_0 = 6.2$, is plotted along the arm length in Fig. 13. The solid line indicates the peak values for the upper arm (I_U^{max}) for different arm length and the dashed line indicates the peak values for the lower arm (I_L^{max}). With increasing the upper arm length, I_U^{max} linearly decreases whereas I_L^{max} linearly increases. This phenomenon has been reported earlier for evanescent modes in one dimension³⁷. We find it to occur even in presence of multiple modes with mixing between the modes. Thus the upper arm and the lower arm behave as classical Ohmic conductors. This is the reason why magnetization curves are so uniform and peak magnetization is always at $\phi/\phi_0 = 6.2$ in Fig. 12. However, absolute quantum behavior can be seen from the fact that the $I_U.l_U + I_L.l_L \neq 0$. For a classical Ohmic resistor doubling of length would have halved the current that helps in defining a material specific resistivity. Such a resistivity cannot be defined for evanescent modes.

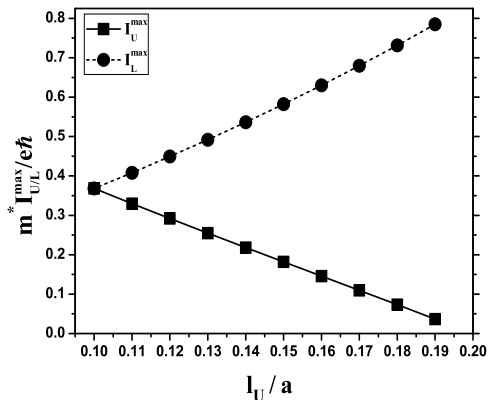


FIG. 13. The figure shows plot of $m^*I_{U/L}^{max}/eh$ obtained at $\phi/\phi_0 = 6.2$ (see Fig. 12) as a function of upper arm length (l_U/a) of the quantum ring. The solid line indicates $m^*I_U^{max}/eh$ as a function of l_U/a and the dashed line indicates $m^*I_L^{max}/eh$ as a function of l_U/a .

The odd current is persistent current which is given by

$$I_{U,L}^{odd} = I_{U,L}(\phi) - I_{U,L}^{even}$$

and plotted as a function of ϕ/ϕ_0 in Fig. 14 for different arm length ratio described in figure caption. The Fig. 14 (a), shows the plot of persistent currents as a function of ϕ/ϕ_0 for the upper arm and Fig. 14 (b) shows the same for the lower arm. The nature of Fig. 14 (a) and (b) remains the same when we change the arm length ratio. The flux value at which the curves peak also remain the same. This is the reason why the total magnetization which is a linear combination of the odd component and even component also remain the same in nature and magnitude as sample parameters and Fermi energy is varied randomly.

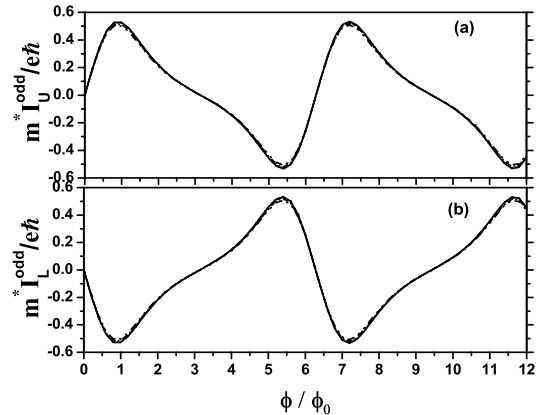


FIG. 14. The figures (a) - (b) show plot of persistent currents in dimensionless unit for the system in Fig. 1 as a function of ϕ/ϕ_0 for different arm lengths keeping the ring length same. In (a) and (b), we have used the same convention and same parameters as in Fig. 12 (a) and (b), respectively.

IV. CONCLUSIONS

Although one-dimensional quantum rings coupled to reservoirs have received a lot of attention in the past, realistic multi-channel rings were never considered. We have considered such a quantum ring coupled to two reservoirs. We have developed the correct formalism to include evanescent modes and multi-channel mixing. Interesting quantum phenomena arise in such systems like persistent currents, circulating currents, Aharonov-Bohm effect in conductance or transport currents. We have studied all these quantum phenomena for a realistic multi-channel ring. Earlier stable quantum switch device was proposed based on evanescent mode conductance and Aharonov-Bohm interferometry^{7,35} (see Fig. 4 and Fig. 12). Internal currents never received any attention and can have equal importance in device application. We have calculated the circulating currents for two different cases. First we have considered two propagating modes along the quantum ring and then we have considered one propagating mode and one evanescent mode along the quantum ring. We cannot get circulating currents using evanescent modes only. We have also calculated magnetization of the quantum ring. Magnetization in quantum ring arises due to two reasons. First is due to transport currents and second is due to Aharonov-Bohm effect. We have calculated strength of magnetization for three different cases, (i) taking two propagating modes, (ii) taking one propagating mode and one evanescent mode and (iii) taking two evanescent modes. For the first two cases we have shown that magnetization behavior is very sensitive for variations in parameters like ring length, arm length, Fermi energy etc, while that for evanescent modes the strength of magnetization ($I_U.l_U + I_L.l_L$) as a function of ϕ/ϕ_0 is same for all variations in system parameters.

Hence there is possibility of robust device action based on magnetic response using evanescent modes only (see Fig. 10, Fig. 11 and Fig. 12).

ACKNOWLEDGMENT

SM and PSD acknowledges Institute of Physics, Bhubaneswar for providing local hospitality where a part of this research work has been done and we all thank DST, India for financial support.

-
- ¹ *Mesoscopic Phenomena in Solids*, edited by B. L. Al'tshuler, R. A. Webb, and P. A. Lee (Elsevier, Amsterdam, 1991).
- ² L. P. Lévy, G. Dolan, J. Dunsmuir, and H. Bouchiat, *Phys. Rev. Lett.* **64**, 2074-2077 (1990).
- ³ V. Chandrasekhar, R. A. Webb, M. J. Brady, M. B. Ketchen, W. J. Gallagher, and A. Kleinsasser, *Phys. Rev. Lett.* **67**, 3578-3581 (1991).
- ⁴ Mailly, D., Chapelier, C., and Benoit, A. *Phys. Rev. Lett.* **70**, 2020-2024 (1993).
- ⁵ P. Singha Deo, V. A. Schweigert, F. M. Peeters and A. K. Geim, *Phys. Rev. Lett.* **79**, 4653-4656 (1997).
- ⁶ Büttiker, M., Imry, Y. and Landauer, R. Josephson behavior in small normal one-dimensional rings. *Phys. Lett.* **96A**, 365-367 (1983).
- ⁷ A. M. Jayannavar and P. S. Deo, *Phys. Rev. B* **51**, 10175-10178 (1995).
- ⁸ S. Datta, *Electronic Transport in Mesoscopic Systems*, Cambridge: Cambridge University Press.
- ⁹ R. S. Popovic, J. A. Flanagan, P. A. Besse, *Sensors and Actuators A* **56**, 39-55 (1995).
- ¹⁰ R. Landauer, *Physics Today* **42**, 119-121 (1989).
- ¹¹ B. C. Gupta, P. Singha Deo and A. M. Jayannavar, *Int. J. Mod. Phys. B* **10**, 3595-3608 (1996).
- ¹² A. M. Jayannavar and P. Singha Deo, *Mod. Phys. Lett. B* **8**, 301-310 (1994).
- ¹³ S. Subramaniam, S. Bandyopadhyay, and W. Porod, *J. Appl. Phys.* **68**, 4861-4870 (1990).
- ¹⁴ S. Datta, M. R. Melloch, S. Bandyopadhyay, R. Noren, M. Vaziri, M. Miller, and R. Reifenberger, *Phys. Rev. Lett.* **55**, 2344-2347 (1985). S. Datta, M. R. Melloch, S. Bandyopadhyay, and M. S. Lundstrom, *Appl. Phys. Lett.* **48**, 487-489 (1986).
- ¹⁵ S. Datta, and B. Das, *Appl. Phys. Lett.* **56**, 665-667 (1990).
- ¹⁶ S. Datta and M. J. McLennan, *Rep. Prog. Phys.* **53**, 1003-1048 (1990).
- ¹⁷ F. Sols, M. Macucci, V. Ravoili, and K. Hess, *Appl. Phys. Lett.* **54**, 350-352 (1989); F. Sols, M. Macucci, V. Ravoili, and K. Hess, *J. Appl. Phys.* **66**, 3892-3906 (1989).
- ¹⁸ B. Molnár, F. M. Peeters and P. Vasilopoulos, *Phys. Rev. B* **69**, 155335, 1-11 (2004).
- ¹⁹ B. Molnár, P. Vasilopoulos and F. M. Peeters, *Appl. Phys. Lett.* **85**, 4 (2004).
- ²⁰ P. Földi, B. Molnár, M. G. Benedict and F. M. Peeters, *Phys. Rev. B* **71**, 033309, 1-4 (2005).
- ²¹ O. Kálmán, P. Földi, M. G. Benedict, F. M. Peeters, *Physica E* **40**, 567-573 (2008).
- ²² S. K. Joshi, D. Sahoo and A. M. Jayannavar, *Phys. Rev. B* **64**, 075320, 1-6 (2001).
- ²³ C. Benjamin and A. M. Jayannavar, *Int. J. Mod. Phys. B* **16**, 1787-1805 (2002).
- ²⁴ H. M. Pastawski, A. Rojo and C. Balseiro, *Phys. Rev. B* **37**, 6246-6250 (1988).
- ²⁵ E. Akkermans, A. Auerbach, J. E. Avron, and B. Shapiro, *Phys. Rev. Lett.* **66**, 76-79 (1991).
- ²⁶ R. Marathe, A. Dhar and A. M. Jayannavar, *Phys. Rev. E* **82**, 031117, 1-4 (2010).
- ²⁷ T. Choi, C. M. Ryu and A. M. Jayannavar, *Int. J. Mod. Phys. B* **12**, 2091 (1998); arxiv: cond-mat/9808245.
- ²⁸ P. Singha Deo and A. M. Jayannavar, *Phys. Rev. B* **50**, 11 629-11 639 (1994).
- ²⁹ P. Singha Deo, B. C. Gupta, A. M. Jayannavar and F. M. Peeters, *Phys. Rev. B* **58**, 10 784-10 788 (1998).
- ³⁰ S. Sengupta Chowdhury, P. Singha Deo, A. K. Roy and M. Manninen, *New Journal of Physics* **10**, 083014, 1-12 (2008).
- ³¹ H. F. Cheung, Y. Gefen, E. K. Riedel, and W. H. Shih, *Phys. Rev. B* **37**, 6050-6062 (1988).
- ³² B. J. van Wees, H. van Houten, C. W. J. Beenakker, J. G. Williamson, L. P. Kouwenhoven, D. van der Marel, and C. T. Foxon, *Phys. Rev. Lett.* **60**, 848-850 (1988).
- ³³ D. A. Wharam, T. J. Thornton, R. Newbury, M. Pepper, H. Ahmed, J. E. Frost, D. G. Hasko, D. C. Peacock, D. A. Ritchie, and G. A. C. Jones, *J. Phys. C* **21**, L209-L214 (1988).
- ³⁴ D. Yu. Sharvin and Yu. V. Sharvin, *JETP Lett.* **34**, 272-275 (1981).
- ³⁵ S. Mukherjee, A. Yadav and P. S. Deo, *Physica E* **47**, 86-94 (2013).
- ³⁶ J. D. Jackson, *Classical Electrodynamics*, third ed., Wiley, New York, (1997).
- ³⁷ T. P. Pareek, P. S. Deo and A. M. Jayannavar, *Phys. Rev. B* **52**, 14 657-14 663 (1995).
- ³⁸ A. M. Jayannavar, P. S. Deo and T. P. Pareek, *Physica B* **212**, 261-266 (1995).
- ³⁹ Su, Y. H., Cho, S. Y., Chen, A. M., and Choi, T., *J. Korean Phys. Soc.* **57** 138-143 (2010).
- ⁴⁰ M. Büttiker, Y. Imry, R. Landauer, and S. Pinhas, *Phys. Rev. B* **31**, 6207-6215 (1985).